Crystallographic Structures of *Discosoma* Red Fluorescent Protein with Immature and Mature Chromophores: Linking Peptide Bond *Trans*−*Cis* Isomerization and Acylimine Formation in Chromophore Maturation[†,‡]

Julie L. Tubbs, John A. Tainer, and Elizabeth D. Getzoff*

Department of Molecular Biology and The Skaggs Institute for Chemical Biology, The Scripps Research Institute, La Jolla, California 92037

Received December 24, 2004; Revised Manuscript Received April 8, 2005

ABSTRACT: The mature self-synthesizing *p*-hydroxybenzylideneimidazolinone-like fluorophores of *Discosoma* red fluorescent protein (DsRed) and *Aequorea victoria* green fluorescent protein (GFP) are extensively studied as powerful biological markers. Yet, the spontaneous formation of these fluorophores by cyclization, oxidation, and dehydration reactions of tripeptides within their protein environment remains incompletely understood. The mature DsRed fluorophore (Gln 66, Tyr 67, and Gly 68) differs from the GFP fluorophore by an acylimine that results in Gln 66 Cα planar geometry and by a Phe 65−Gln 66 *cis* peptide bond. DsRed green-to-red maturation includes a green-fluorescing immature chromophore and requires a chromophore peptide bond *trans*−*cis* isomerization that is slow and incomplete. To clarify the unique structural chemistry for the individual immature "green" and mature "red" chromophores of DsRed, we report here the determination and analysis of crystal structures for the wild-type protein (1.4 Å resolution), the entirely green DsRed K70M mutant protein (1.9 Å resolution), and the DsRed designed mutant Q66M (1.9 Å resolution), which shows increased red chromophore relative to the wild-type DsRed. Whereas the mature, red-fluorescing chromophore has the expected *cis* peptide bond and a sp^2-hybridized Gln 66 Cα with planar geometry, the crystal structure of the immature green-fluorescing chromophore of DsRed, presented here for the first time, reveals a *trans* peptide bond and a sp^3-hybridized Gln 66 Cα with tetrahedral geometry. These results characterize a GFP-like immature green DsRed chromophore structure, reveal distinct mature and immature chromophore environments, and furthermore provide evidence for the coupling of acylimine formation with *trans*−*cis* isomerization.

Discosoma red fluorescent protein (RFP), known commercially as DsRed, complements the homologous and widely used *Aequorea victoria* green fluorescent protein (GFP)[1] as a fluorescent tag for protein localization, gene expression, fluorescence resonance energy transfer (FRET), and cell-based screening of small compounds in drug development (*1*, *2*). GFP and DsRed fluorescence emission arises within the folded protein from a spontaneously formed *p*-hydroxybenzylideneimidazolinone (GFP) or derivative (DsRed) fluorophore that is a posttranslational modification of an internal tripeptide sequence (Ser 65-Tyr 66-Gly 67 for GFP; Gln 66-Tyr 67-Gly 68 for DsRed) (*3*, *4*). The structures of the GFP (*5*, *6*) and the red-emitting DsRed (*4*, *7*, *8*) chromophores are known, but the order of reactions and mechanistic biosynthetic reactions for chromophore formation have yet to be established. GFP chromophore formation is accomplished by cyclization through nucleophilic attack of the Gly nitrogen atom on the Ser carbonyl carbon atom, dehydration of the Ser carbonyl oxygen atom, and oxidation (GFP oxidation) at the Tyr Cα−Cβ bond (*3*, *9*) (Figure 1A). DsRed chromophore formation likely goes through a GFP-like chromophore intermediate that has been proposed to form by the same mechanism as for the GFP chromophore (*4*, *10*). The mature red-fluorescing chromophore for DsRed has undergone an additional oxidation reaction (DsRed oxidation) relative to the green-fluorescing chromophore of GFP, resulting in a double bond between the Gln 66 N and Cα atoms (*4*) (Figure 1B). To rationally and successfully design improved DsRed, GFP, and homologous fluorescent proteins as molecular tags for which specific properties can be controlled, we must first more fully understand chromophore formation and maturation. For this reason, knowing the structures of distinct chromophore maturation states and intermediates would be invaluable.

DsRed is initially green fluorescent (480 nm excitation; 500 nm emission) and slowly develops red fluorescence (558 nm excitation; 583 nm emission), reaching half its maximal red fluorescence in about 27 h (*11*). The mature red-emitting

[†] This work was supported by National Institutes of Health Grant GM 37684 (E.D.G.), National Institutes of Health Ruth L. Kirschstein National Research Service Award (J.L.T.), and The Skaggs Institute for Chemical Biology Skaggs Predoctoral Fellowship (J.L.T.).

[‡] Atomic coordinates have been deposited with the Protein Data Bank (PDB; http://www.rcsb.org/pdb) at the Research Collaboratory for Structural Bioinformatics (RCSB; http://pdb.rutgers.edu) under PDB codes 1ZGO for wild-type DsRed, 1ZGP for DsRed K70M, and 1ZGQ for DsRed Q66M.

* To whom correspondence should be addressed. Phone: (858) 784-2878. Fax: (858) 784-2289. E-mail: edg@scripps.edu.

[1] Abbreviations: DsRed, *Discosoma* red fluorescent protein; FRET, fluorescence resonance energy transfer; GFP, *Aequorea victoria* green fluorescent protein; asCP, *Anemonia sulcata* chromoprotein; KFP, *Anemonia sulcata* kindling fluorescent protein; eqFP611, *Entacmaea quadricolor* fluorescent protein; rtms5, *Montipora efflorescens* fluorescent protein; mRFP1, *Discosoma* monomeric red fluorescent protein.

10.1021/bi0472907 CCC: $30.25
Published on Web 06/30/2005

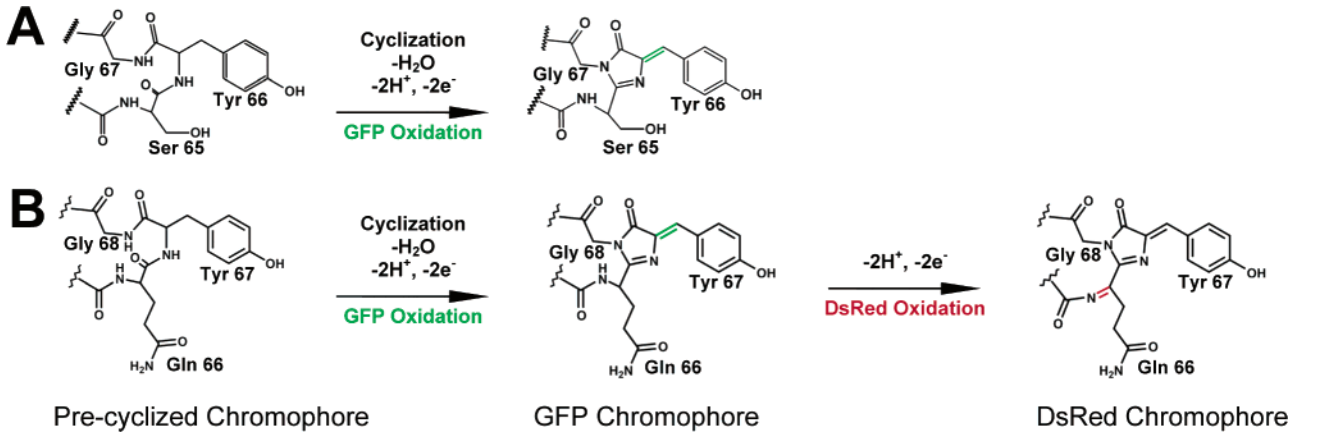

FIGURE 1: GFP (A) and DsRed (B) chromophore formation. The double bond resulting from GFP oxidation (green) and the distinct double bond resulting from DsRed oxidation (red) reveal the key differences between GFP and DsRed chromophores. As crystal structures do not generally distinguish protonation states, this figure does not attempt to address differing ideas in the literature regarding chromophore protonation states during the various stages of chromophore formation.

("red") DsRed chromophore, for which the structure is known, has extended conjugation from the green-emitting GFP chromophore through an acylimine substituent (*4*). The acylimine (−C═N−C═O) includes the main chain carbonyl group of Phe 65 conjugated with Gln 66 N and Cα atoms and accounts for the red-shifted fluorescence spectra (*4*). The chromophore of mature DsRed differs from that of GFP by the presence of both an acylimine and an unusual *cis* peptide bond linkage between Phe 65 and Gln 66 (*7*). The significance of the *cis* peptide bond in DsRed chromophore maturation and its possible coupling with acylimine formation have not been determined. The structure of the immature green-emitting ("green") DsRed chromophore is unknown but is proposed to be equivalent to the structure for the GFP chromophore, based on its spectroscopic properties and mass spectrometry (*4*). The green DsRed chromophore can be seen spectroscopically as a 480 nm shoulder to the peak for the red-emitting chromophore at 558 nm in the absorbance and fluorescence excitation spectra (*11*).

DsRed green-to-red maturation remains incomplete, even upon prolonged aging (*4*, *11*), with nearly 50% of chromophores estimated to remain green (*4*). Gross et al. (*4*) have cautioned that, unless fitted into electron density as a superposition of two chromophores, a stochastic mixture of approximately equimolar amounts of the two chromophores within a crystal structure could obscure bond angles. As a result, resolution of individual chromophore types within a mixture can be tricky and requires diffraction data of sufficient quality and resolution. Yet, the published coordinates (1.9 Å resolution; PDB codes 1G7K and 1GGX) for the wild-type DsRed crystal structures (*7*, *8*) surprisingly assume all red chromophores within their models with Phe 65 C−Gln 66 N−Gln 66 Cα peptide bond angles that range from 140° to 165°.

To characterize the unique environments and structures for the individual immature green and mature red chromophores of DsRed, we determined crystal structures of the wild-type protein to 1.4 Å resolution and the DsRed variants K70M (1.9 Å resolution), which remains entirely green, and Q66M (1.9 Å resolution), which has a reduced green absorbance relative to red. These direct structural data reported here support a GFP-like immature green DsRed chromophore, reveal insights into the distinct mature and immature chromophore environments, and provide evidence for the coupling of acylimine formation with *trans*−*cis* isomerization.

EXPERIMENTAL PROCEDURES

Site-Directed Mutagenesis, Expression, and Purification. DsRed (Clontech) was subcloned into a pET15 vector (Novagen), which contains an N-terminal 6× His tag. Mutations were introduced into DsRed by QuikChange site-directed mutagenesis (Stratagene). DsRed protein was expressed at 37 °C in 9 L cultures of *Escherichia coli* BL21(DE3) RIL (Stratagene) cells. Cells were induced with 0.2 mM isopropyl β-D-thiogalactoside (IPTG) when they reached an optical density of 0.4, then grown for 12−16 h, and pelleted by centrifugation. Cell pellets were resuspended in sonication buffer (50 mM Tris, pH 8.0, 300 mM NaCl, 10 mM imidazole) and lysed by sonication. The soluble portion of the lysate, which contained the DsRed protein, was purified by Ni-NTA agarose (Qiagen) column chromatography and the 6× His tag cleaved by digestion with α-chymotrypsin, as previously described (*7*). Purified DsRed protein was buffer exchanged using a PD-10 column (Amersham Biosciences) into 20 mM Hepes, pH 8.0, and 300 mM NaCl, concentrated to 15−40 mg/mL, flash frozen in 50 μL aliquots in liquid nitrogen, and stored at −80 °C.

Crystallization and X-ray Diffraction Data Collection. Crystals were grown by the sitting drop vapor diffusion method using 1 μL of protein at 15 mg/mL in 20 mM Hepes, pH 8.0, 300 mM NaCl, and 1 μL of well solution. Crystals of wild-type DsRed protein were grown from well solution containing 52−62% 2-methyl-2,4-pentanediol (MPD) and 100 mM Hepes, pH 7.0, and diffraction data were collected at ALS beamline 5.0.1 on a ADSC CCD Quantum 210 detector (see Table 1). DsRed Q66M crystals were grown from well solution containing 14% PEG 8000, 50 mM NaCl, and 100 mM phosphate−citrate, pH 4.2. DsRed K70M crystals were grown from well solution containing 15% PEG 4000, 200 mM $MgCl_2$, and 100 mM citrate, pH 6.5. Q66M and K70M crystals were briefly transferred to a 20% ethylene glycol in mother liquor solution for cryoprotection and frozen in liquid nitrogen immediately prior to diffraction data collection at ALS beamlines 8.3.1 and 8.2.1, respectively, on a ADSC CCD Quantum 210 detector (see Table 1).

Table 1: Crystallographic Data Collection and Refinement Statistics

crystallographic data			
protein	DsRed wild type	DsRed K70M	DsRed Q66M
space group	$P2_1$	$P1$	$P2_1$
unit cell dimensions	$a = 55.7$, $b = 127.2$, $c = 57.1$ Å; $\beta = 100.4°$	$a = 57.3$, $b = 57.2$, $c = 71.5$ Å; $\alpha = 89.7$, $\beta = 100.2$, $\gamma = 92.9°$	$a = 74.2$, $b = 88.0$, $c = 161.6$ Å; $\beta = 96.7°$
molecules per asymmetric unit	4	4	8
X-ray source	ALS beamline 5.0.1	ALS beamline 8.2.1	ALS beamline 8.3.1
wavelength (Å)	1.000	1.000	0.999
data range (Å) (last shell)	40−1.40 (1.45−1.40)	50−1.90 (1.97−1.90)	40−1.90 (1.97−1.90)
observations (unique)	363894 (148353)	93451 (59952)	317097 (157512)
completeness (%) (last shell)	96.8 (93.2)	85.7 (85.1)	97.0 (88.6)
R_{sym}[a] (last shell)	5.1 (35.7)	7.2 (25.4)	6.4 (41.7)
$I/\sigma I$ (last shell)	18 (1.9)	6 (2.2)	10 (1.8)
refinement			
resolution (Å)	40−1.40	50−1.90	40−1.90
reflections $F > 0$ (cross-validation)	132400 (7039)	54675 (2903)	141168 (7494)
non-hydrogen atoms (solvent molecules)	7219 (541)	7160 (510)	14320 (1655)
R_{cryst}[b] (R_{free}[c])	14.3 (20.6)	22.6 (26.5)	19.3 (22.2)
rms bond length (Å)	0.010	0.013	0.013
rms bond angles (deg)	0.030 Å[d]	1.7	1.7

[a] R_{sym} = the unweighted R value on I between symmetry mates. [b] $R_{cryst} = \sum_{hkl}||F_o(hkl)| - |F_c(hkl)||/\sum_{hkl}|F_o(hkl)|$. [c] R_{free} = the cross-validation R factor for 5% of reflections against which the model was not refined. [d] For structures refined in Shelx-97, bond angles are reported as distances between the first and third atoms.

Diffraction data were processed with DENZO and Scalepack (*12*). Structures were solved by molecular replacement with AMoRe (*13*), using wild-type DsRed (PDB code 1G7K) (*8*) with the chromophore omitted as a search model.

Crystallographic Refinement. Crystallographic refinement was done with CNS (*14*) for the DsRed K70M and Q66M variants and Shelx-97 (*15*) for wild-type DsRed. Xfit (*16*) was used for manual model building into $2F_o - F_c$ and composite omit and simulated annealing omit $2F_o - F_c$ and $F_o - F_c$ electron density maps. Chromophores were built into the model after two rounds of refinement. Chromophore restraints were generated as described in the Supporting Information. Water molecules were added to regions of greater than 3σ positive density in a $F_o - F_c$ difference map after two rounds of refinement. Structural superpositions were done with Sequoia (*17*). To determine percentages for mature and immature chromophores, occupancies for chromophore atoms were refined with Shelx-97 as described in the Supporting Information.

Spectroscopy. Solution absorbance measurements were made on a Hewlett-Packard scanning UV−visible spectrophotometer, model 8453. Fluorescence measurements were made on a Jobin Yvon (Spex) Fluoromax-3 fluorometer. All solution measurements were made at 22 °C. DsRed Q66M solution absorbance samples were diluted into 50 mM citrate, pH 4.5, and 300 mM NaCl. Fluorescence samples were diluted into 20 mM Hepes, pH 8.0, and 300 mM NaCl. Wild-type DsRed fluorescence excitation and emission measurements were made using 583 nm emission and 558 nm excitation wavelengths, respectively. DsRed Q66M fluorescence excitation and emission measurements were made using 587 nm emission and 565 nm excitation wavelengths, respectively. Single crystal absorbance spectra were measured from crystals flash frozen in a stream of nitrogen gas (100 K) on a home-built microspectrophotometer based upon an earlier design (*18*).

RESULTS

High-Resolution Crystal Structure of Wild-Type DsRed. To resolve the mixture of mature and immature structures for each chromophore within the DsRed tetramer, we solved the crystal structure of the wild-type DsRed protein to 1.4 Å resolution (Table 1). The electron density shows a mixture of two chromophore populations (Figure 2A) for each of the four DsRed subunits. The mature, red-fluorescing chromophore has a *cis* peptide bond and a sp^2-hybridized Gln 66 Cα with planar geometry (Figure 2B), as previously reported (*7*, *8*). A second chromophore population has a *trans* peptide bond and a sp^3-hybridized Gln 66 Cα with tetrahedral geometry (Figure 2C). This matches the GFP chromophore structure and is therefore presumably responsible for the green fluorescence. Crystallographic refinement of chromophores with hybrid features, i.e., combining a planar Gln 66 Cα and a *trans* Phe 65−Gln 66 peptide bond, or a tetrahedral Gln 66 Cα and a *cis* peptide bond, produces distorted peptide bond and chromophore geometries (data not shown), indicating that these chromophore forms are incompatible with our structural data.

Due to the high resolution of the diffraction data, we were able to obtain accurate occupancies for the mature and immature chromophore populations. Both refine to approximately 50% for each of the four chromophores within the tetramer (see Supporting Information), in agreement with data from mass spectrometry (*4*), sodium dodecyl sulfate−polyacrylamide gel electrophoresis (*4*), and single molecule spectroscopy (*19*). The *trans*−*cis* isomerization difference between the green and red chromophores about the Phe 65−Gln 66 peptide bond is accompanied by an approximate 35° rotation of the Phe 65 carbonyl within the plane of the peptide bond (Figure 2A). In addition, to accommodate the change in Gln 66 Cα geometry, the Gln 66 $\chi 1$ torsion angles differ by about 25°. The Gln 66 Cβ atoms for the two chromophore types are positioned about 0.7 Å apart, whereas the remainder of the Gln 66 side chain from Cγ to the amide is unchanged. Therefore, the crystallographic data indicate that red and green DsRed chromophores differ both by Gln 66 Cα geometry and Phe 65−Gln 66 peptide bond conformation.

The Green Chromophore Structure of DsRed K70M. To confirm the structure of the immature DsRed chromophore

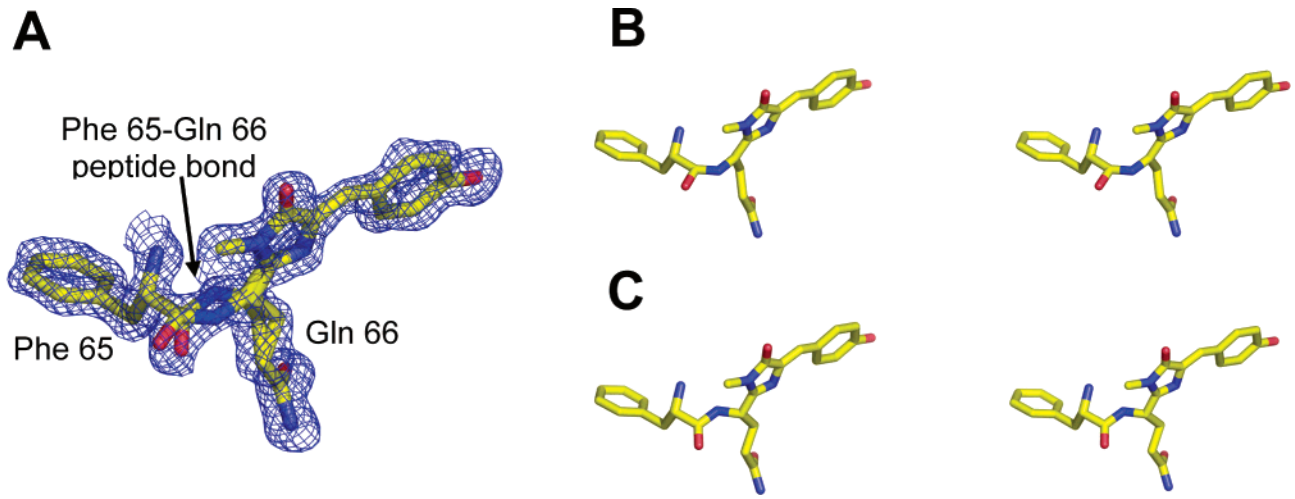

FIGURE 2: Refined high-resolution DsRed structure revealing *trans* and *cis* chromophore conformations. DsRed wild-type chromophore with $2F_o - F_c$ electron density omit map contoured at 1σ (A). Electron density supports both *trans* and *cis* Phe 65−Gln 66 peptide bonds. The Gly 68 carbonyl carbon and oxygen atoms are not shown. Stereoview of the mature red (B) and immature green (C) chromophores. Gln 66 Cα (center) is sp^2-hybridized with planar geometry in (B) and sp^3-hybridized with tetrahedral geometry in (C). Oxygen atoms are colored red and nitrogen atoms blue.

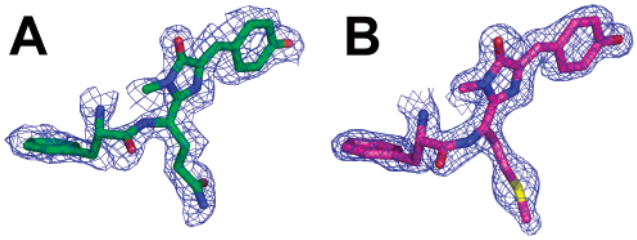

FIGURE 3: DsRed green and red chromophore states by designed mutations. DsRed K70M (A) and Q66M (B) chromophore structures and $2F_o - F_c$ omit electron density contoured at 1σ. For K70M, the Gln 66 Cα atom displays tetrahedral geometry and the Phe 65−Gln 66 peptide bond is in the *trans* conformation (A). For Q66M, the Met 66 Cα atom displays trigonal geometry and the Phe 65−Met 66 peptide bond is in the *cis* conformation (B).

and its protein environment, we crystallized and determined the 1.9 Å resolution structure for the DsRed mutant K70M (Table 1), which was shown by Baird et al. (*11*) to dominantly exhibit an immature green chromophore. The immature chromophore of the DsRed K70M structure exhibits tetrahedral geometry for the Gln 66 Cα atom and the *trans* conformation for the Phe 65−Gln 66 peptide bond (Figure 3A), matching the green chromophore from the high-resolution wild-type DsRed structure (Figure 2C). The wild-type and K70M crystal structures both show that the planar conjugated π-system of the DsRed immature chromophore, for which crystallographic data have previously been unavailable, is structurally identical to that of the *A. victoria* GFP chromophore.

The Red Chromophore Structure of DsRed Q66M. To better define the structure of a DsRed variant with the fully matured red chromophore, we determined the crystal structure of the DsRed Q66M variant to 1.9 Å resolution (Table 1). The excitation shoulder for DsRed Q66M (490 nm) corresponding to the green chromophore is reduced in comparison to wild type (480 nm), indicating a higher percentage of red chromophores (Figure S2a) for this variant. The Q66M mutation also tested our hypothesis that the significantly red-shifted absorbance of methionine-containing chromophores in DsRed homologues, such as *Entacmaea quadricolor* eqFP611 (*20*), resulted primarily from this single sequence difference. As we predicted, DsRed Q66M exhibits a red shift from the wild-type protein in absorbance and fluorescence excitation (565 nm) and emission (587 nm) wavelengths (Figure S2a).

The crystallographic structure of DsRed Q66M shows that the chromophore has cyclized and matured through both oxidations (Figure 3B). The DsRed oxidation is evident from the planar geometry of the Met 66 Cα atom and the *cis* configuration of the Phe 65−Met 66 peptide bond (Figure 3B), which match the high-resolution wild-type red chromophore structure (Figure 2B). The extended side chain conformation of Met 66 resembles that of the wild-type Gln 66. Q66M chromophore maturation is complete for seven of eight chromophores in the two tetrameric protein molecules of this crystal structure (see Supporting Information), providing an excellent opportunity to examine the "all-red" chromophore environment. Comparison of single crystal and solution absorbance spectra (Figure S2b) indicates that the Q66M crystal structure is representative of the protein in solution.

Examination of Red and Green Chromophore Environments. To examine the structural chemistry associated with DsRed chromophore maturation, we compared and contrasted features of the chromophore environment among the seven mature red chromophores of the Q66M DsRed structure and the four cyclized, but immature green chromophores of the K70M DsRed structure (Figure 4). The overall protein fold and assembly of DsRed remain unchanged by mutation and maturation of the chromophore, as do the positioning of the chromophores within the protein subunits and the assembly of the tetramers. Subunits for both Q66M and K70M DsRed align with only 0.2−0.3 Å root mean square deviations (rmsd) in the Cα position from those of the four wild-type subunits, compared with roughly 0.1−0.2 Å rmsd among the eight Q66M DsRed structures and 0.2 Å rmsd among the four K70M DsRed structures. Thus, our results show that the changes between DsRed variants with mature versus immature chromophores are localized to the chromophores and their environment.

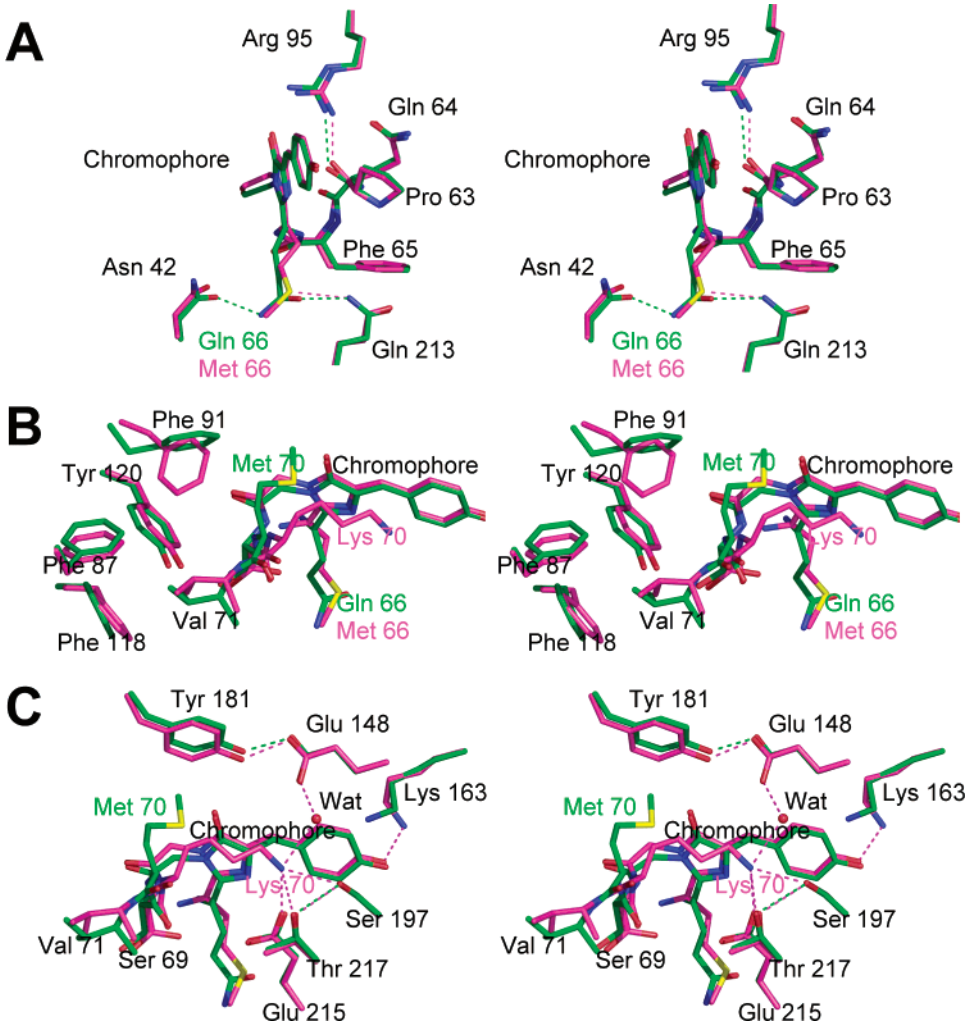

FIGURE 4: Distinct environments for red and green chromophores in DsRed by designed mutations. Stereoviews and overlays of DsRed Q66M (purple) and K70M (green) chromophores and surrounding environments. Oxygen atoms are colored red, nitrogen atoms blue, and sulfur atoms yellow. Water molecules are shown as red spheres and hydrogen bonds as dashed lines.

In the red Q66M chromophore environment (Figure 4A), Met 66 aligns with the wild-type Gln 66 side chain conformation and maintains the hydrogen bond with Gln 213, but not with Asn 42. The Gln 213 hydrogen bond helps to align the 66 side chain correctly for the *cis* conformer of the 65−66 peptide bond of the mature DsRed chromophore. In Q66M DsRed, the side chain of Asn 42 is rotated roughly 20° in $\chi 2$ from its wild-type position to form a hydrogen bond to the Glu 215 carbonyl O, in addition to the wild-type hydrogen bonds with the side chains of Glu 215 and Ser 69. Preceding the chromophore, the Pro 63 carbonyl angles about 20° closer to Arg 95, allowing a better hydrogen bond with the Arg guanidinium group.

In the green K70M chromophore environment (Figure 4B,C), the side chain of Met 70 diverges from that of the wild-type Lys 70; the Cα−Cβ vector of Met 70 is rotated roughly 45° relative to the Cα−Cβ vector of Lys 70. The side chain of Met 70 is somewhat disordered except for the sulfur atom, which is positioned just above the Ser 69 backbone. To make room for the side chain of Met 70, the Phe 91 side chain rearranges significantly (Figure 4B). In addition, the backbone atoms for residues 69 through 75 move outward approximately 0.3−1.3 Å, away from the chromophore and toward the wall of the β-barrel, with the largest movements for residues 69−71 (Figure 4B,C). To accommodate these shifts, the side chains of Phe 87, Phe 118, and Tyr 120 change their tilt (Figure 4B). The K70M substitution eliminates the side chain hydrogen-bonding network from the Lys 70 NZ atom to Ser 197, Glu 215, Thr 217, and a water molecule and then propagates to Glu 148 and Tyr 181 (Figure 4C). Also, the Lys 163 side chain is in two conformations: in one, the terminal NZ makes a hydrogen bond with the chromophore's phenolic oxygen as observed in wild type and Q66M; in the other, NZ points almost 180° in the opposite direction (Figure 4C). The K70M chromophore environment is clearly perturbed by the substitution of Lys with Met.

DISCUSSION

Knowing the structures of distinct DsRed chromophore maturation states is fundamental to fully understanding chromophore formation and to the successful design of improved DsRed, GFP, and homologous fluorescent proteins as molecular tags with specific predetermined properties. The DsRed crystal structures reported here clarify that the immature green DsRed and GFP chromophores have identically conjugated systems, highlight distinctions between mature and immature DsRed chromophore environments, and support coupling of acylimine formation with *trans*−*cis* peptide isomerization. Our structures help to resolve key

questions regarding chromophore maturation by revealing four major points concerning green and red states of DsRed and the roles of specific residues and features in chromophore maturation.

First, the mature red and immature green chromophores differ both by Gln 66 Cα geometry (to accommodate the oxidation state of the Gln 66 N−Cα bond) and by Phe 65−Gln 66 peptide bond conformation. The crystal structure of the green DsRed mutant K70M provides the first direct crystallographic structural evidence that the green species spectroscopically observed in DsRed is indeed the GFP chromophore. This result is consistent with mass spectrometry conclusions for the chromophore of green DsRed mutant K83R (*4*). The comparison of wild-type, K70M, and Q66M crystal structures shows that *trans*−*cis* peptide bond isomerization is unique to the mature red chromophore and is likely coupled to the acylimine-forming DsRed oxidation (see below).

Second, the structure of the K70M variant provides a basis to investigate the puzzling role of Lys 70 in chromophore maturation. The similar length of Met and Lys side chains argues against a steric role. Although the new conformation of this side chain in the K70M structure does lead to structural rearrangements (Figure 4B,C), no steric impacts on the chromophore are obvious. Instead, we favor a role for the positive charge of Lys 70 in chromophore maturation. Interestingly, the K70R mutant, like DsRed wild type, matures from green to red (*11*). In a recently proposed mechanism for the chromophore DsRed oxidation reaction, Lys 70, through a salt bridge interaction, was suggested to maintain an anionic Glu 215 (*8*). However, the equivalent Lys in DsRed homologue eqFP611, which also has an acylimine-containing chromophore, does not participate in this salt bridge (*21*). An alternative role for the positive charge of Lys (and Arg) 70 in DsRed green-to-red maturation arises from its position near the chromophore.

To further analyze the significance of the Lys 70 positive charge near the chromophore, we examined crystal structures of three DsRed homologues with red-shifted fluorescence emission: naturally occurring proteins eqFP611 from *E. quadricolor* (PDB code 1UIS) (*21*) and Rtms5 from *Montipora efflorescens* (PDB code 1MOU) (*22*), and the engineered kindling fluorescent protein (KFP) derived from *Anemonia sulcata* chromoprotein (asCP) (PDB code 1XQM) (*23*). Two of these proteins, eqFP611 and Rtms5, undergo chromophore acylimine formation to form DsRed-like chromophores. The KFP chromophore has a *p*-hydroxybenzylideneimidazolinone core as observed for other GFP-like protein chromophores but undergoes fragmentation at the peptide bond preceding the chromophore, resulting in an imino substituent rather than an acylimine. Both eqFP611 and KFP have Lys at the DsRed Lys 70 position. Rtms5 has Ile at this position, but the guanidinium group of a neighboring Arg (corresponding to DsRed Ser 197) is located near where the Lys terminal amine would be and therefore seems to provide a compensating positive charge. [For eqFP611 and KFP, the side chain of a histidine at position 197 participates in a $\pi-\pi$ stacking interaction with the chromophore phenolate ring.] Interestingly, each of these positively charged functional groups, DsRed Lys NZ, eqFP611 Lys NZ, KFP Lys NZ, and the Rtms5 Arg guanidinium group, is positioned near the chromophore phenolate ring to create a cation$-\pi$ interaction. Cation$-\pi$ interactions occur frequently in proteins and provide stabilization energy comparable to salt bridge interactions (*24*). These interactions include not only the positively charged amino acids Lys and Arg, but also residues that carry a partial positive charge on the amino group of the side chain, such as Asn and Gln (specifically called amino$-\pi$ interactions) (*25*).

On the basis of these observations and our structures presented here, we propose that the positive charge of the lysine side chain acts to further stabilize a chromophore with greater electron delocalization than for GFP, as is the case for the mature red DsRed chromophore. This could explain why replacement of positive Lys 70 with neutral and hydrophobic Met results in a green protein that never becomes red. In GdFP, a gold-fluorescing variant of GFP, an amino$-\pi$ interaction is observed between the amino-substituted tryptophan, replacing the chromophore tyrosine, and a nearby Phe (Ile 161 in DsRed) (*26*). The amino$-\pi$ interaction was proposed to promote more efficient charge transfer in the chromophore excited state and could play a similar role in DsRed. Alternatively, for DsRed, the cation$-\pi$ interaction may stabilize charge on the chromophore to lower excited-state energy, in a role similar to that of $\pi-\pi$ stacking of the chromophore tyrosyl moiety with a nearby tyrosine in the yellow-fluorescing variant of GFP (*27*). The proposed cation$-\pi$ or amino$-\pi$ interaction for chromophore stabilization could also explain the wild-type-like maturation kinetics for the DsRed K70Q variant (our unpublished data). Interestingly, in wild-type GFP the Gln that corresponds to DsRed Lys 70 is directed away from an amino$-\pi$ interaction with the chromophore by differences between the hydrogen-bonding environments of DsRed and GFP.

Another possible explanation for the inability of DsRed K70M to mature to a red-emitting form is the lack of two distinct conformations for its Ser 69 side chain, in contrast to the wild-type and Q66M proteins. Yarbrough and coworkers (*8*) proposed a catalytic role for Ser 69 in DsRed acylimine formation, based on their proximity. Gurskaya et al. (*28*) supported this role by the introduction of some red fluorescence in a double mutant (Asn to Ser at this position and Ile to Ser at a position distant from the chromophore) of cyan fluorescent dsFP483 from *Discosoma* sp. However, the single Asn to Ser mutant at the Ser 69 equivalent position of this DsRed homologue showed only cyan fluorescence. Furthermore, the S69A mutant of DsRed still exhibits both red and green fluorescence (our unpublished data). Our data, therefore, show that DsRed Ser 69 is not essential for DsRed acylimine formation, although it likely enhances the efficiency of this process. Thus, we propose that DsRed K70M remains green due to the lack of a positive charge at position 70 rather than the conformation of the Ser 69 side chain.

Third, the Q66M variant raises the questions of why its chromophores fully mature and why its spectroscopic features are more red shifted than those of the wild-type protein (Figure S2a). One possible explanation for why Q66M chromophores mature more fully derives from the chromophore structure. A major distinguishing feature of the mature from the immature DsRed chromophore is the Phe 65−Gln 66 *cis* peptide bond. Several stabilizing factors for the *cis* conformation of the peptide bond have been proposed, including the delocalization of the electrons of the Gln 66 main chain into the chromophore's molecular orbitals (*7*).

Met contains a sulfur and is therefore more electron-rich than Gln. The increased availability of electrons may help to stabilize the *cis* peptide bond conformation for the Q66M variant. Alternatively, the Met at position 66 may position the side chain properly for acylimine formation, through preferential hydrogen bonding of its electron-rich sulfur atom with the electron-deficient NE2 atom of Gln 213, rather than with the electron-rich OD1 atom of Asn 42.

The red shift of Q66M spectroscopic properties in comparison to those of wild type can likely be attributed to the interactions of the methionine with surrounding residues. Other proteins homologous to DsRed and with Met at the first position of the chromophore include *A. sulcata* asCP and its KFP variant and *E. quadricolor* eqFP611. Like DsRed Q66M, all of the proteins, asCP, KFP, and eqFP611, have fluorescence emission that is redshifted in comparison to that of wild-type DsRed. The wavelengths for absorbance and fluorescence emission of asCP (47% homology to DsRed) resemble those of DsRed Q66M, with absorption at 568 nm (565 nm for DsRed Q66M) and emission at 595 nm for the wild-type protein or at 600 nm for its KFP variant (587 nm for DsRed Q66M) (*29*−*31*). The eqFP611 protein (48.4% homology to DsRed) absorbs similarly to wild-type DsRed but emits at 611 nm due to a larger Stokes shift (*20*). Crystal structures for the KFP and eqFP611 proteins reveal different chromophore conjugation and pathways for chromophore maturation for KFP versus DsRed and eqFP611. Comparison of the chromophore environments in crystal structures of eqFP611 (*21*) and DsRed Q66M (Figure 4) reveals some similarities. The carbonyl of eqFP611 Thr 60, equivalent to DsRed Pro 63, angles upward to better hydrogen bond with Arg 95, as observed for DsRed Q66M. Also, the extended conformation of the eqFP611 chromophore Met is similar to that seen for DsRed Q66M, and the sulfur hydrogen bonds to Gln 213. Hydrogen bonds and other polar interactions involving Met sulfurs are not very common (*32*−*34*), and participation of the chromophore Met sulfur atoms of DsRed Q66M and eqFP611 in a hydrogen bond with a nearby residue may in part be responsible for the spectral red shifts. Furthermore, several engineered monomeric variants of DsRed derived from monomeric RFP (mRFP1) contain the Q66M mutation, which red shifts the excitation and emission spectra relative to mRFP1 (*35*), thereby supporting the proposal that methionine at position 66 is responsible for the red shifts.

Fourth, the order of the DsRed oxidation and peptide bond isomerization reactions was not previously clear. Are acylimine formation and peptide bond isomerization linked? In argument against their coupling, Yarbrough et al. (*8*) concluded in a note added in proof that the immature chromophore contains a *cis* peptide bond. Similarly, a theoretical study concluded that the immature chromophore contains a *cis* peptide bond, and as a result, *trans*−*cis* isomerization cannot be responsible for the green to red maturation of DsRed (*36*). In contrast, our crystallographic structures unambiguously show that the green chromophores of both K70M (Figure 3A) and immature DsRed (Figure 2C) have a *trans* Phe 65−Gln 66 peptide bond. Trigonal Gln 66 Cα geometry requires a *cis* peptide bond, while tetrahedral Gln 66 Cα geometry requires a *trans* peptide bond for the least surrounding structural disruption within the DsRed protein scaffold during peptide bond isomerization. This is due to the restrictions for trigonal and tetrahedral Gln 66 Cα geometry (e.g., the requirement for the Gln 66 N and Cβ atoms to be coplanar with a trigonal Gln 66 Cα atom) and geometrical constraints imposed by the helical secondary structure and surrounding environment (e.g., consistency of Phe 65 and chromophore location with electron density and proper peptide geometry). Although the results presented here do not conclusively order the maturation processes, together they argue that DsRed oxidation is coupled to peptide bond isomerization.

In sum, these combined structural, mutational, and spectroscopic analyses of DsRed characterize the structural chemistry of distinct mature and immature chromophores and their protein environments. The immature green-fluorescing chromophore differs from the mature red-fluorescing chromophore by a *trans* peptide bond and a sp^3-hybridized Gln 66 Cα with tetrahedral geometry. In contrast to previous proposals, our results argue that the *trans*−*cis* isomerization is linked to acylimine formation, forming the key step in DsRed chromophore maturation.

ACKNOWLEDGMENT

Many thanks to K. Hitomi for critical reading of the manuscript, to A. Arvai, R. Brudler, D. Shin, E. Garcin, and U. Genick for helpful suggestions and discussions, and to the staff at The Advanced Light Source where crystallographic diffraction data were collected. The Advanced Light Source is supported by the Director, Office of Science, Office of Basic Energy Sciences, Materials Sciences Division, of the U.S. Department of Energy under Contract DE-AC03-76SF00098 at Lawrence Berkeley National Laboratory.

SUPPORTING INFORMATION AVAILABLE

Method for generating chromophore restraints for crystallographic refinement, crystallographic refinement of occupancy for chromophore atoms, Table S1 (a list of DsRed chromophore restraints for Shelx-97), Figure S1 (bond angles for refinement of a Gln 66 Cα atom with ideal tetrahedral or ideal planar geometry and DsRed chromophore atoms for which occupancies were refined), and Figure S2 (comparison of DsRed Q66M and wild-type fluorescence and solution and crystal absorbance spectra). This material is available free of charge via the Internet at http://pubs.acs.org.

REFERENCES

1. Haugwitz, M., Dery, O., Turpin, P., and Fang, Y. (2003) Applications of novel fluorescent proteins; Assay tutorial: NFPs permit more sophisticated cell-based screening capabilities, in *Genet. Eng. News 23*, 36−39.
2. Verkhusha, V., and Lukyanov, K. A. (2004) The molecular properties and applications of Anthozoa fluorescent proteins and chromoproteins, *Nat. Biotechnol. 22*, 289−296.
3. Tsien, R. Y. (1998) The green fluorescent protein, *Annu. Rev. Biochem. 67*, 509−544.
4. Gross, L. A., Baird, G. S., Hoffman, R. C., Baldridge, K. K., and Tsien, R. Y. (2000) The structure of the chromophore within DsRed, a red fluorescent protein from coral, *Proc. Natl. Acad. Sci. U.S.A. 97*, 11990−11995.
5. Ormo, M., Cubitt, A. B., Kallio, K., Gross, L. A., Tsien, R. Y., and Remington, S. J. (1996) Crystal structure of the *Aequorea victoria* green fluorescent protein, *Science 273*, 1392−1395.
6. Yang, F., Moss, L. G., and Philips, G. N., Jr. (1996) The molecular structure of green fluorescent protein, *Nat. Biotechnol. 14*, 1246−1251.

7. Wall, M. A., Socolich, M., and Ranganathan, R. (2000) The structural basis of red fluorescence in the tetrameric GFP homolog DsRed, *Nat. Struct. Biol. 7*, 1133−1138.
8. Yarbrough, D., Wachter, R. M., Kallio, K., Matz, M. V., and Remington, S. J. (2001) Refined crystal structure of DsRed, a red fluorescent protein from coral, at 2.0-Å resolution, *Proc. Natl. Acad. Sci. U.S.A. 98*, 462−467.
9. Barondeau, D. P., Putnam, C. D., Kassmann, C. J., Tainer, J. A., and Getzoff, E. D. (2003) Mechanism and energetics of green fluorescent protein chromophore synthesis revealed by trapped intermediate structures, *Proc. Natl. Acad. Sci. U.S.A. 100*, 12111−12116.
10. Verkhusha, V. V., Chudakov, D. M., Gurskaya, N. G., Lukyanov, S., and Lukyanov, K. A. (2004) Common pathway for the red chromophore formation in fluorescent proteins and chromoproteins, *Chem. Biol. 11*, 845−854.
11. Baird, G. S., Zacharias, D. A., and Tsien, R. Y. (2000) Biochemistry, mutagenesis, and oligomerization of DsRed, a red fluorescent protein from coral, *Proc. Natl. Acad. Sci. U.S.A. 97*, 11984−11989.
12. Otwinowski, Z., and Minor, W. (1997) Processing of X-ray diffraction data collected in oscillation mode, *Methods Enzymol. 276*, 307−326.
13. Navaza, J. (1994) AMoRe: An automated package for molecular replacement, *Acta Crystallogr. A 50*, 157−163.
14. Brünger, A. T., Adams, P. D., Clore, G. M., DeLano, W. L., Gros, P., Grosse-Kunstleve, R. W., Jiang, J. S., Kuszewski, J., Nilges, M., Pannu, N. S., Read, R. J., Rice, L. M., Simonson, T., and Warren, G. L. (1998) Crystallography & NMR system: A new software suite for macromolecular structure determination, *Acta Crystallogr. D 54*, 905−921.
15. Sheldrick, G. M., and Schneider, T. R. (1997) SHELXL: High-resolution refinement, *Methods Enzymol. 277*, 319−343.
16. McRee, D. M. (1999) XtalView/Xfit-A versatile program for manipulating atomic coordinates and electron density, *J. Struct. Biol. 125*, 156−165.
17. Bruns, C. M., Hubatsch, I., Ridderstrom, M., Mannervik, B., and Tainer, J. A. (1999) Human glutathione transferase A4−4 crystal structures and mutagenesis reveal the basis of high catalytic efficiency with toxic lipid peroxidation products, *J. Mol. Biol. 288*, 427−439.
18. Hadfield, A., and Hajdu, J. (1993) A fast and portable microspectrophotometer for protein crystallography, *J. Appl. Crystallogr. 26*, 839−842.
19. Garcia-Parajo, M. F., Koopman, M., van Dijk, E. M. H. P., Subramaniam, V., and van Hulst, N. F. (2001) The nature of fluorescence emission in the red fluorescent protein DsRed, revealed by single-molecule detection, *Proc. Natl. Acad. Sci. U.S.A. 98*, 14392−14397.
20. Wiedenmann, J., Schenk, A., Rocker, C., Girod, A., Spindler, K.-D., and Nienhaus, G. U. (2002) A far-red fluorescent protein with fast maturation and reduced oligomerization tendency from *Entacmaea quadricolor* (Anthozoa, Actinaria), *Proc. Natl. Acad. Sci. U.S.A. 99*, 11646−11651.
21. Petersen, J., Wilmann, P. G., Beddoe, T., Oakley, A. J., Devenish, R. J., Prescott, M., and Rossjohn, J. (2003) The 2.0-Å crystal strucuture of eqFP611, a far red fluorescent protein from the sea anemone *Entacmaea quadricolor*, *J. Biol. Chem. 278*, 44626−44631.
22. Prescott, M., Ling, M., Beddoe, T., Oakley, A. J., Dove, S., Hoegh-Glulberg, O., Devenish, R. J., and Rossjohn, J. (2003) The 2.2 Å crystal structure of a pocilloporin pigment reveals a nonplanar chormophore conformation, *Structure 11*, 275−284.
23. Wilmann, P. G., Petersen, J., Devenish, R. J., Prescott, M., and Rossjohn, J. (2005) Variations on the GFP chromophore: A polypeptide fragmentation within the chromophore revealed in the 2.1 Å crystal structure of a nonfluorescent chromoprotein from Anemonia sulcata, *J. Biol. Chem. 280*, 2401−2404.
24. Burghardt, T. P., Juranic, N., Macura, S., and Ajtai, K. (2002) Cation-π interaction in a folded polypeptide, *Biopolymers 63*, 261−272.
25. Biot, C., Buisine, E., and Rooman, M. (2003) Free-energy calculations of protein-ligand cation-π and amino-π interactions: From vacuum to proteinlike environments, *J. Am. Chem. Soc. 125*, 13988−13994.
26. Bae, J. H., Rubini, M., Jung, G., Wiegand, G., Seifert, M. H. J., Azim, M. K., Kim, J.-S., Zumbusch, A., Holak, T. A., Moroder, L., Huber, R., and Budisa, N. (2003) Expansion of the genetic code enables design of a novel "gold" class of green fluorescent proteins, *J. Mol. Biol. 328*, 1071−1081.
27. Wachter, R. M., Elsliger, M. A., Kallio, K., Hanson, G. T., and Remington, S. J. (1998) Structural basis of spectral shifts in the yellow-emission variants of green fluorescent protein, *Structure 6*, 1267−1277.
28. Gurskaya, N. G., Savitsky, A. P., Yanushevich, Y. G., Lukyanov, S. A., and Lukyanov, K. A. (2001) Color transitions in coral's fluorescent proteins by site-directed mutagenesis, *BMC Biochem. 2*, 6.
29. Lukyanov, K. A., Fradkov, A. F., Gurskaya, N. G., Matz, M. V., Labas, Y. A., Savitsky, A. P., Markelov, M. L., Zaraisky, A. G., Zhao, X., Fang, Y., Tan, W., and Lukyanov, S. A. (2000) Natural animal coloration can be determined by a nonfluorescent green fluorescent protein homolog, *J. Biol. Chem. 275*, 25879−25882.
30. Wiedenmann, J., Elke, C., Spindler, K.-D., and Funke, W. (2000) Cracks in the beta-can: Fluorescent proteins from *Anemonia sulcata* (Anthozoa, Actinaria), *Proc. Natl. Acad. Sci. U.S.A. 97*, 14091−14096.
31. Chudakov, D. M., Belousov, V. V., Zaraisky, A. G., Novoselov, V. V., Staroverov, D. B., Zorov, D. B., Lukyanov, S., and Lukyanov, K. A. (2003) Kindling fluorescent proteins for precise in vivo photolabeling, *Nat. Biotechnol. 21*, 191−194.
32. Ippolito, J. A., Alexander, R. S., and Christianson, D. W. (1990) Hydrogen bond stereochemistry in protein structure and function, *J. Mol. Biol. 215*, 457−471.
33. Gregoret, L. M., Rader, S. D., Fletterick, R. J., and Cohen, F. E. (1991) Hydrogen bonds involving sulfur atoms in proteins, *Proteins 9*, 99−107.
34. Pal, D., and Chakrabarti, P. (2001) Non-hydrogen bond interactions involving the methionine sulfur atom, *J. Biomol. Struct. Dyn. 19*, 115−128.
35. Shaner, N. C., Campbell, R. E., Steinbach, P. A., Giepmans, B. N. G., Palmer, A. E., and Tsien, R. Y. (2004) Improved monomeric red, orange and yellow fluorescent proteins derived from Discosoma sp. red fluorescent protein, *Nat. Biotechnol. 22*, 1567−1572.
36. Zaveer, M. S., and Zimmer, M. (2003) Structural analysis of the immature form of the GFP homologue DsRed, *Bioorg. Med. Chem. Lett. 13*, 3919−3922.

BI0472907